JMEPEG (2012) 21:1708–1713
DOI: 10.1007/s11665-011-0077-z
©ASM International
1059-9495/$19.00

Effects of Temperature on Microstructure and Wear of Salt Bath Nitrided 17-4PH Stainless Steel

Jun Wang, Yuanhua Lin, Hongyuan Fan, Dezhi Zeng, Qian Peng, and Baoluo Shen

(Submitted October 3, 2010; in revised form October 17, 2011)

Salt bath nitriding of 17-4 PH martensitic precipitation hardening stainless steels was conducted at 610, 630, and 650 °C for 2 h using a complex salt bath heat-treatment, and the properties of the nitrided surface were systematically evaluated. Experimental results revealed that the microstructure and phase constituents of the nitrided surface alloy are highly process condition dependent. When 17-4PH stainless steel was subjected to complex salt bathing nitriding, the main phase of the nitrided layer was expanded martensite (α'), expanded austenite (γ_N), CrN, Fe_4N, and $(Fe,Cr)_xO_y$. In the sample nitrided above 610 °C, the expanded martensite transformed into expanded austenite. But in the sample nitrided at 650 °C, the expanded austenite decomposed into α_N and CrN. The decomposed α_N then disassembled into CrN and alpha again. The nitrided layer depth thickened intensively with the increasing nitriding temperature. The activation energy of nitriding in this salt bath was 125 ± 5 kJ/mol.

Keywords 17-4PH stainless steel, complex salt bath nitriding, microstructure, temperature, wear property

1. Introduction

The type of 17-4 precipitation hardening (17-4 PH) stainless steel is widely used as a structural material for chemical and power plants, such as light water reactors (LWRs) and pressurized water reactors (PWRs), due to its high strength, high fracture toughness, good weldability, and ease of machinability (Ref 1, 2). However, its wider application is restricted by it poor tribological properties, which have necessitated the development of advanced surface engineering technologies to address the problem (Ref 3, 4).

Nitriding of 17-4PH steel stems back to 1985 when Tesi et al. (Ref 5) studied plasma nitriding of 17-4PH as a complementary treatment to age hardening. Significant surface hardening was achieved, which is in line with most research on plasma and gas nitriding of stainless steel (Ref 6-12). Moreover, the previous study suggests that the performance of surface corrosion-resistance provided by complex salt bath heat-treatment is better than that provided by hard chrome plating or other galvanic layers (Ref 13). Besides, it was reported that a corrosion-resistance compound layer, could be further improved when dipped to an oxidizing salt melt (Ref 14). Consequently, Li and Yeung et al. (Ref 15) claimed that the complex salt bath process is considered as an effective engineering technology to improve corrosion properties. It is an environment-friendly process that originates from salt bath nitriding technology where a combination of high fatigue resistance and good wear and corrosion resistance can be achieved.

But little knowledge exists of the effects of temperature on microstructure and wear behavior when complex salt bath nitriding is done on 17-4PH stainless steel. Therefore, the aim of the study is to investigate the influence of nitriding temperature on surface microstructure of 17-4PH stainless steel, mainly using X-ray diffraction (XRD); scanning electron microscopy (SEM), equipped energy dispersive analysis system of X-ray (EDS), and transmission electron microscopy (TEM).

2. Experiment

The samples were prepared from grade 17-4PH stainless steel with the composition shown in Table 1. Each sample of the martensitic precipitation hardening stainless steel was solid solution treated at 1040 °C for half an hour and then tempered at 595 °C for 4 h. All of the flat surfaces of each sample were ground and polished to a mirror finish and then ultrasonically cleaned. The samples of 17-4PH steel nitriding were dipped in molten salt at 610-650 °C for 2 h and then cooled in warm water to room temperature. The nitriding salts with a special formula contain a certain oxidization agent developed by Chengdu Tool Institute. A detailed description of the complex process can be found in the literature (Ref 14).

The structural changes in the modified layer were investigated using cross sections for optical microscopy and the Type JSM5910-LV scanning electron microscopy with the Philips EDS tester. X-ray diffractometer type Dmax-1400 with Cu Kα radiation and a nickel filter was used to determine the phases present in the modified layer. Microstructural studies were performed in a Philips TECNAI 20 TEM operating at an accelerating voltage of 200 kV.

Jun Wang, Hongyuan Fan, and **Baoluo Shen**, School of Manufacturing Science and Engineering, Sichuan University, Chengdu 610065, People's Republic of China; **Qian Peng**, National Key Laboratory for Nuclear Fuel and Materials, Nuclear Power Institute of China, Chengdu 610041, People's Republic of China; **Yuanhua Lin** and **Dezhi Zeng**, State Key Laboratory of Oil and Gas Reservoir Geology and Exploitation, Southwest Petroleum University, Chengdu 610500, People's Republic of China. Contact e-mail: scutg@163.com.

Table 1 Chemical composition of type 17-4PH stainless steel (mass%)

Elements	C	Si	Mn	P	S	Cr	Ni	Cu	Nb	Fe
%	0.04	0.6	0.3	0.023	0.013	16.39	4.32	3.4	0.36	Bal.

Dry-sliding tribological tests were performed using a rotational speed of 200 rpm for duration of 3600 s. A normal operating load of 30 N was used. For the counter body, 50-mm-diameter GCr15 rings were selected. The wear loss was measured by Type TG328A photoelectron analytical balance with an accuracy of 0.1 mg.

3. Results and Discussion

3.1 Metallography

It was observed that the microstructure produced during salt bath nitriding of 17-4PH stainless steel changed according to treatment temperature, as shown in Fig. 1. Optical microscopy (OM) and SEM observations showed that the formed nitrided layers were etched at 610 and 650 °C respectively, but the substrate was not. It can be seen from the optical micrograph shown in Fig. 1(a) that the depth of the total nitrocarburized layer is approximately 94 μm. The nitrided layers are distinguished from the substrate due to the etching degree being different.

A typical cross-sectional microstructure of 650 °C/2 h salt bath nitrided specimens from the SEM is depicted in Fig. 1, showing that the nitrided layer can be divided into four zones. These are defined as the external zone, the medial zone, the transition zone of nitriding layers and the substrate (denoted as '1, 2, 3, 4' in Fig. 1(b), respectively).

3.2 Phase Analysis of the Nitriding Layer in 17-4PH SS

Figure 2 shows the XRD patterns at the nitrided and untreated samples. The phase composition of nitrided layers on 17-4 PH steel depends on nitriding temperature and nitrogen potential. As depicted in the figure, the phases present in the untreated 17-4PH are dominated by martensite (α′) with a small quantity of retained austenite (γ). After complex nitriding treatment at 610 °C for 2 h, the sample microstructure is characterized by peaks of expanded martensite (α_N), chromium nitride (CrN), and γ′-Fe_4N, and a small amount of expended austenite (γ′), which is in line with the observations by Sun and Bell (Ref 10) and Li (Ref 14).

Figure 3 displays the EDS of a cross section of the complex nitrided sample in Fig. 1(b) (650 °C for 2 h). The external zone of the layer from the high temperature process is rich in chromium and oxygen (black arrowed in Fig. 3). The medial zone of the nitriding layer is rich in iron and nitrogen, while poor in chromium. But the transition zone is rich in chromium and nitrogen, while poor in iron. According to the EDS and XRD of the edge area of the tested samples, it is evident that the edge layer of about 10 μm depth after nitriding treatment is composed of chromium iron oxide ($(Cr,Fe)_xO_y$) and γ′-Fe_4N. Next to it is a Fe_4N layer of 5 μm thickness, then, a lightly etched zone of about 45 μm depth, which is mainly composed of CrN. At a depth greater than 60 μm, the main microstructure of nitrided layer is α'_N-expanded martensite, which shows that

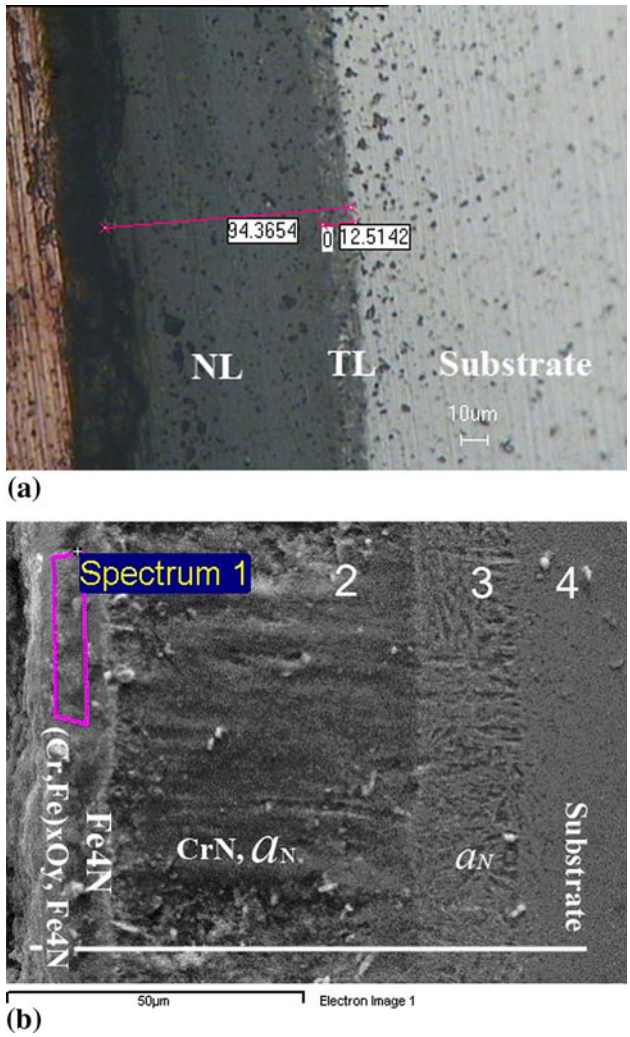

Fig. 1 Optical metallography (a) of 17-4PH SS under various salt baths nitrided at 610 °C and SEM (b) of 17-4PH SS under various salt baths nitrided at 650 °C (NL: nitrided layer; TL: transition layer)

the martensite is supersaturated with nitrogen atoms. From Fig. 1(b), it is obvious that the slightly etched area in this inner zone, which is probably due to the CrN precipitation and in the transition zone of nitriding layers, i.e., the α'_N zone, has a better resistance to corrosion than the CrN zone. Besides, after complex nitriding at 650 °C, the copper atom in nitrided layer was moved from the external zone to the medial zone and the transition zone of nitriding layers (Fig. 3), which is in line with Kochmański's observation (Ref 12).

3.3 The Effect of the Temperature on the Nitriding Microstructure

XRD diffraction patterns of phase structure of the layers at different temperatures are shown in Fig. 4. It can be clearly seemed that a set of α-Fe peaks for the unnitrided sample (denoted as '000' in Fig. 4) is very strong. Meanwhile, the austenite peak is not clear, indicating that it is present in only a small amount. Detailed microstructure of untreated 17-4PH SS could be found in previous studies (Ref 1, 2). After nitriding, XRD pattern of the samples was dramatically changed for different nitriding temperatures, showing the importance of the effect of temperature.

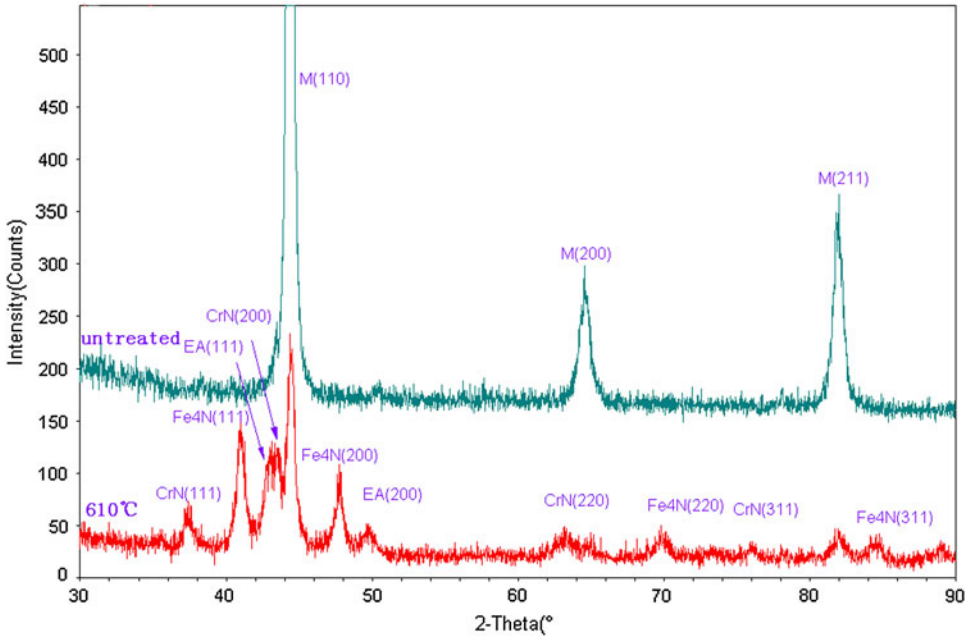

Fig. 2 The XRD profiles of 17-4PH SS under various salt bath nitrided conditions

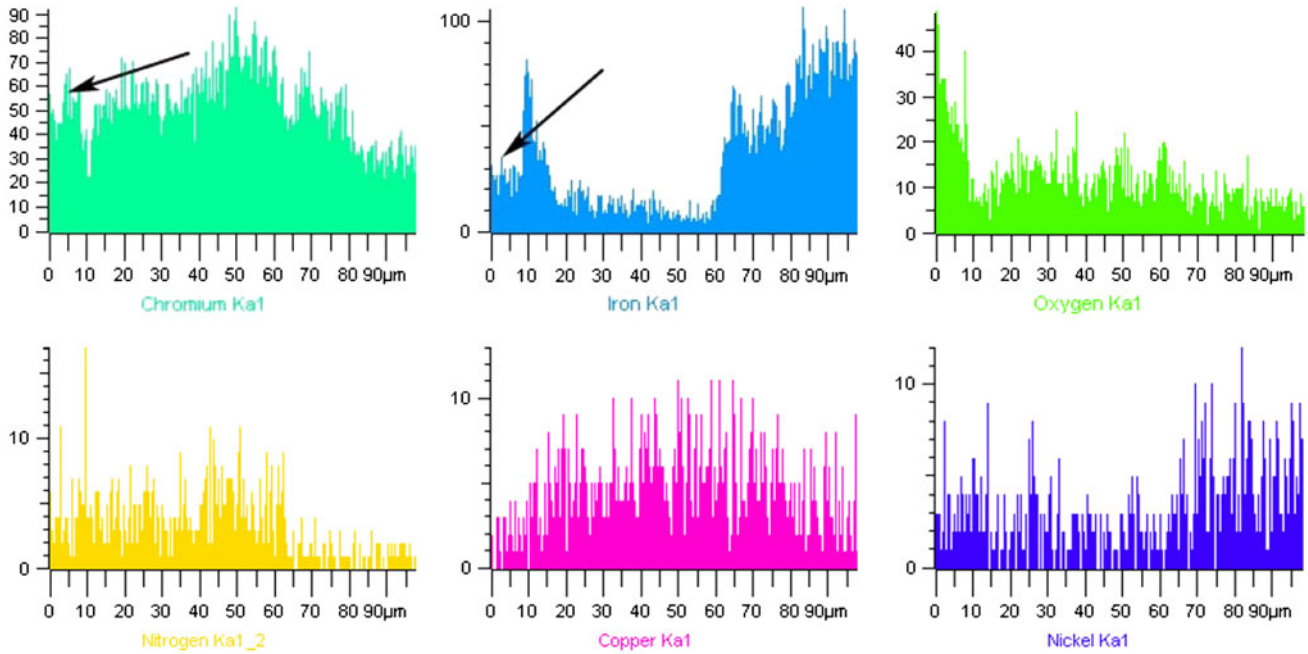

Fig. 3 EDS results of Fig. 1(b) in 17-4PH SS nitrided at 650 °C

XRD results show the peaks of α-Fe in the 17-4PH steel declined after nitriding at 610 °C, and diffraction patterns of expended austenite appeared, which is in line with Dong's observation by TEM (Ref 11). Since nitrogen is an 'austenite stabiliser' and the nitrogen-rich layer tends to appear in the form of an f.c.c. structure rather than a b.c.c. structure, the alpha (b.b.c.) grains are prone to transforming to f.c.c. grains during the nitriding treatment (Ref 16). When the nitrogen diffuses inwards, the f.c.c. grain lattice is supersaturated by nitrogen to such extent that the transformation of alpha into expended austenite, i.e., γ_N occurs (Ref 17). Therefore, nitriding at 610 and 630 °C produces a noticeable peak at a diffraction angle 2θ of 42°, 49°, and 73°, corresponding with (111), (200), and (220) crystal planes of austenite. This has been associated with a metastable phase called expanded austenite (denoted as EA in Fig. 4). Also it is called S-phase (Ref 8, 9, 13), and is observable together with peaks of the α_N (nitrogen-containing martensite supersaturated by nitrogen). The diffraction peaks of α_N were weakened, which indicates that most martensite was transformed into austenite in the form of expanded austenite, especially at 630 °C. Moreover, the expanded austenite also can be formed from the pre-existent retained austenite (Ref 11).

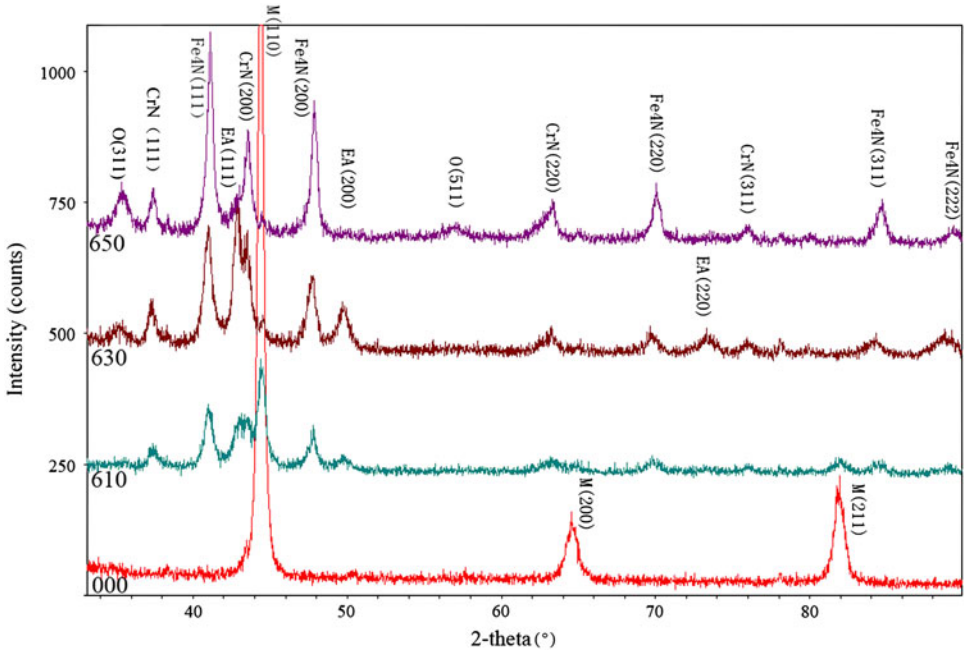

Fig. 4 XRD profiles of 17-4PH SS under various salt bath nitrided conditions

However, the expanded austenite peaks disappeared at 650 °C. Meanwhile, the CrN peaks are sharpened in (111) and (220) crystal planes. The reason is probably that the precipitation of CrN depletes chromium of the expanded austenite phase, favoring the formation of a mixed layer of α_N and CrN ($\gamma_N \rightarrow \alpha_N$ + CrN). So the diffraction peak of γ_N disappears. It has been reported that Cr nitride formation is favored due to its high negative enthalpy and low Cr diffusivity in the matrix at temperature higher than 450 °C (Ref 18). Dong observed this transformation by TEM in 17-4PH plasma nitriding at high temperature (Ref 11). Therefore, for the samples nitrided at 650 °C, there is no evidence of γ_N, but CrN is abundant. The reason for the peaks of α_N is not clear, but possibly they are due to the decomposition of α_N into alpha and CrN ($\alpha_N \rightarrow \alpha$ + CrN). So the set of CrN peaks for the high temperature nitrided sample is very strong.

From the diffraction patterns (Fig. 4), differences in nitride γ'-Fe_4N diffraction peaks intensities are observable. It is obvious that higher peaks correspond to higher nitriding temperatures, and the chromium iron oxide (denoted as O in Fig. 4) diffraction peak intensity increased as the nitrided temperature increased. Above 610 °C, with increasing nitriding temperature, the diffusivity of nitrogen and oxygen atoms in the nitriding agent increases. So there are more nitrides and oxides, such as Fe_4N, CrN, and $(Fe,Cr)_xO_y$ produced and the depth of nitrided layer is greater.

Furthermore, from Fig. 4, it is can be concluded that the martensite (alpha) diffraction peak did not shift after nitriding, which shows that the lattice parameter of alpha was unchanged. When the steel was nitrided at a certain high temperature, the copper precipitates from martensite (shown in Fig. 5), which would cause its lattice to decrease (Ref 19, 20). At the same time the nitrogen and carbon atoms from nitriding agent diffuse into steel surface and enlarge the lattice. If the increment of alpha lattice parameter caused by nitrogen and carbon atoms just makes up for the decrement by copper precipitated during nitriding, the martensite lattice changes little during the process. The copper distribution changes in the nitrided layer in Fig. 3, which is evidence of copper being precipitated from the supersaturated substrate.

The relations of nitrided layer depth to the treating temperature are shown in Fig. 6. From the figure, it is very clear that the thickness of nitrided layers of 17-4 PH steel obtained at a temperature higher than 600 °C, is a linear function of temperature, and increases intensively with the increasing temperature. This may be ascribed to the faster diffusion of atoms at higher temperature.

Figure 7 shows the plot of layer thickness [$\ln(d^2)$] against inverse temperature ($1/T$) for complex nitriding. In this plot the slope of the straight line gives the activation energy for the diffusion process. The activation energy is independent of nitriding time and was determined to be 124 ± 5 kJ/mol. This is in good agreement with the result of Dimitrov et al. (Ref 21) who calculated effective activation energy of 121 kJ/mol, but slightly larger than that of Menthe et al. (Ref 22) who determined activation energy of 104 kJ/mol for plasma nitriding in AISI 304L SS.

3.4 Hardness and Wear Behavior

Figure 8 shows that the micro-hardness of nitrided layers as a function of temperature and very steep micro-hardness increasing was found on the sample surface. The maximum values measured from the treated surface are observed to be approximate 1100 $HV_{0.1}$ at 610 °C, which is about 3.7 times as hard as the untreated material (309 $HV_{0.1}$). This dramatic increase in hardness is probably due to the formation of Cr nitrides. The decrease in surface hardness at higher temperature (650 °C) was accompanied by the formation of a significant amount of CrN phase (Ref 22).

Dry-sliding wear loss data of the unnitrided and nitrided 17-4PH SS layers are shown in Fig. 9. According to the figure, the dry-sliding wear rate of the nitrided layers is only about 5-10% that of the unnitrided substrate. It can be concluded from these data that the dry-sliding wear rate of nitrided 17-4PH SS

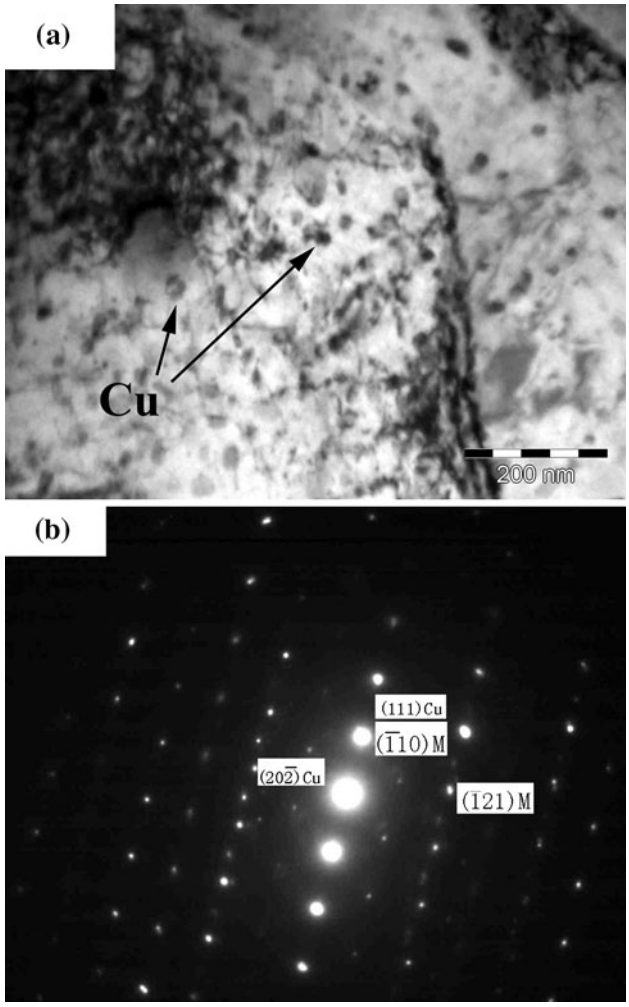

Fig. 5 Morphology of the 17-4PH SS matrix after nitriding treated 610 °C (a) martensite matrix and ε-Cu, (b) SADP of (a)

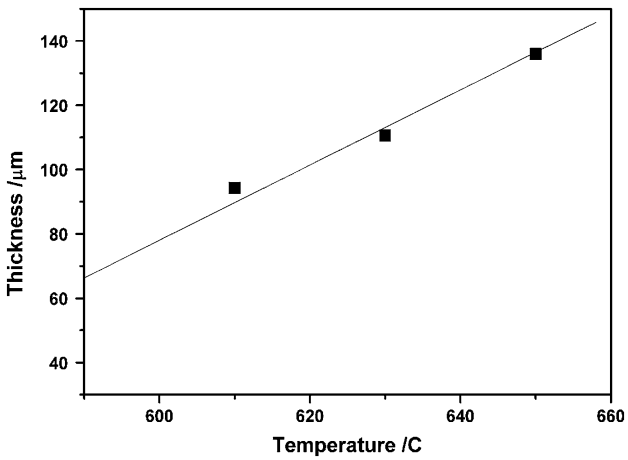

Fig. 6 Change of nitrided layer thickness with nitrided temperature in 17-4PH SS

depends closely on the nitriding temperature. A hard α_N and/or γ_N layer can probably be attributed to a minimum value at 630 °C. In addition, an increasing formation of Cr nitrides and chromium iron oxide in the case with temperature increasing is

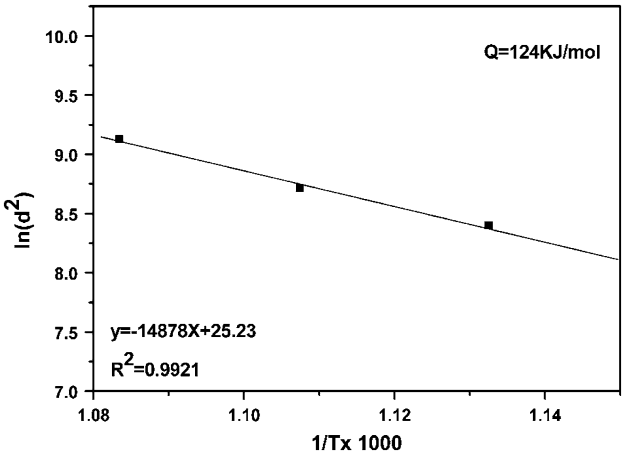

Fig. 7 Relationship of ln d^2 with inverse temperature ($1/T$)

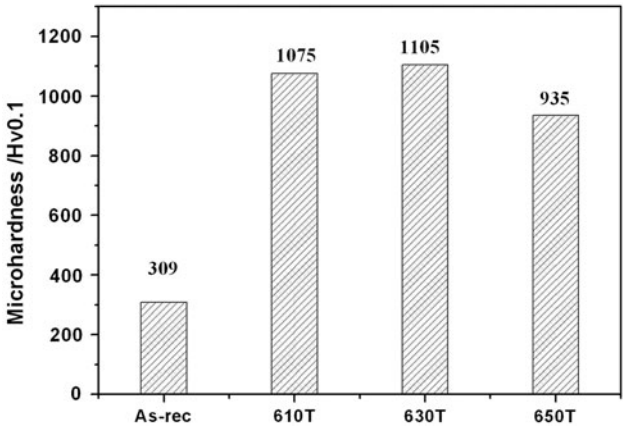

Fig. 8 Microhardness of 17-4PH SS plasma nitrided at various temperatures

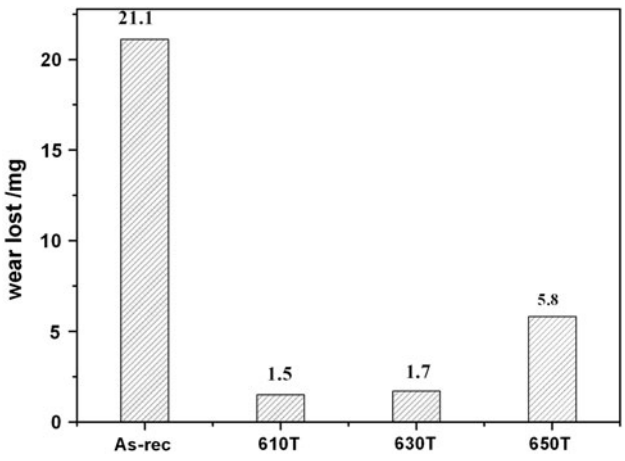

Fig. 9 The effect of temperature on wear behavior of 17-4PH SS

probably the cause of the dry-sliding wear resistance decreasing. More Cr nitrides existing in the layer deteriorated dry-sliding wear resistance of 17-4PH steel, The dry-sliding wear loss of nitrided steel reaches a maximum value at 650 °C where a single chromium iron oxide nitride layer is produced. Moreover, the dry-sliding wear resistance of the nitrided layer

formed at 610 °C is higher than that at other temperatures, which is most probably due to presence of a small quantity of chromium iron oxide that has excellent wear resistance.

4. Conclusion

When 17-4PH stainless steel was subjected to complex salt bathing nitriding, the main phase of the nitrided layer was expanded martensite (α'), expanded austenite (γ_N), CrN, Fe_4N, and $(Fe,Cr)_xO_y$. In the sample nitrided above 610 °C, the expanded martensite transformed into expanded austenite. But in the sample nitrided at 650 °C, the expanded austenite decomposed into α_N and CrN. The decomposed α_N then disassembled into CrN and alpha again. The nitrided layer depth thickened intensively with the increasing nitriding temperature. The activation energy of nitriding in this salt bath was 125 ± 5 kJ/mol. All treatments can effectively improve the surface hardness and the sliding wear resistance under unlubricated conditions.

Acknowledgments

The authors are very grateful to the National Natural Science Foundation of China (Grant No. 50901047), the Ph.D. Programs Foundation of Ministry of Education of china (Grant No. 2008006101051) for financial support of this research work. And the author (J.W.) would like to thank Prof. Xiong Ji of Sichuan University, China for their valuable discussions during the course of the research.

References

1. W. Jui Hung and L. Chih Kuang, Influence of High Temperature Exposure on the Mechanical Behavior and Microstructure of 17-4 PH Stainless Steel, *J. Mater. Sci.*, 2003, **38**, p 965
2. J. Wang, H. Zou, X. Wu, and C. Li, The Effect of Long-Term Isothermal Aging on Dynamic Fracture Toughness of Type 17-4 PH SS at 350°C, *Mater. Trans.*, 2005, **46**, p 846
3. A. Leyland, D.B. Lewis, P.R. Stevenson, and A. Matthews, Low Temperature Plasma Diffusion Treatment of Stainless Steels for Improved Wear Resistance, *Surf. Coat. Technol.*, 1993, **62**, p 608
4. F. Alonso, A. Arizaga, A. Garcia, and J.I. Onate, Tribological Effects of Yttrium, Nitrogen Ion Implantation on a Precipitation Hardening Stainless Steel, *Surf. Coat. Technol.*, 1994, **66**, p 291
5. B. Tesi, T. Bacci, and G. Poli, Analysis of Surface Structures and of Size and Shape Variations in Ionitrided Precipitation Hardening Stainless Steel Samples, *Vacuum*, 1985, **35**(8), p 307
6. Y. Sun and T. Bell, Plasma Surface Engineering of a Low-Alloy Steel, *Mater. Sci. Eng. A*, 1991, **140**, p 419
7. Y. Sun, T. Bell, and G. Wood, Wear Behaviour of Plasma-Nitrided Martensitic Stainless Steel, *Wear*, 1994, **178**, p 131
8. D. Manova, G. Thorwarth, S. Mandl, H. Neumann, B. Stritzker, and B. Rauschenbach, Variable Lattice Expansion in Martensitic Stainless Steel After Nitrogen Ion Implantation, *Nucl. Instrum. Methods B*, 2006, **242**, p 285
9. R.B. Frandsen, T. Christiansen, and M.A.J. Somers, Simultaneous Surface Engineering, Bulk Hardening of Precipitation Hardening Stainless Steel, *Surf. Coat. Technol.*, 2006, **200**, p 5160
10. Y. Sun and T. Bell, Low Temperature Plasma Nitriding Characteristics of Precipitation Hardening Stainless Steel, *Surf. Eng.*, 2003, **19**(5), p 331
11. H. Dong, M. Esfandiari, and X.Y. Li, On the Microstructure and Phase Identification of Plasma Nitrided 17-4PH Precipitation Hardening Stainless Steel, *Surf. Coat. Technol.*, 2008, **202**, p 2969
12. P. Kochmański and J. Nowacki, Activated Gas Nitriding of 17-4PH Stainless Steel, *Surf. Coat. Technol.*, 2006, **200**, p 6558
13. K. Marusic, H. Otmacic, D. Landek, and F. Cajner, Modification of Carbon Steel Surface by the Tenifer® Process of Nitrocarburizing and Post-oxidation, *Surf. Coat. Technol.*, 2006, **201**, p 3415
14. H.Y. Li, D.F. Luo, C.F. Yeung, and K.H. Lau, Advanced QPQ Complex Salt Bath Heat Treatment, *J. Mater. Process. Technol.*, 1997, **69**, p 45
15. C.F. Yeung, K.H. Lau, H.Y. Li, and D.F. Luo, Microstructural Studies of QPQ Complex Salt Bath Heat-Treated Steels, *J. Mater. Process. Technol.*, 1997, **66**, p 249
16. C. Blawert, A. Weisheit, B.L. Mordike, and R.M. Knoop, Plasma Immersion Ion Implantation of Stainless Steel: Austenitic Stainless Steel in Comparison to Austenitic-Ferritic Stainless Steel, *Surf. Coat. Technol.*, 1996, **85**, p 15–27
17. B. Larisch, U. Brusky, and H.J. Spies, Plasma Nitriding of Stainless Steels at Low Temperatures, *Surf Coat Technol.*, 1999, **116–119**, p 205
18. C.E. Foerster, F.C. Serbena, S.L.R. da Silva, C.M. Lepienski, C.J. de M. Siqueira, and M. Ueda, Mechanical and Tribological Properties of AISI 304 Stainless Steel Nitrided by Glow Discharge Compared to Ion Implantation and Plasma Immersion Ion Implantation, *Nucl. Instrum. Methods B*, 2007, **257**, p 732
19. K. Stiller, M. Hattestrand, and F. Danoix, Precipitation in 9Ni-12Cr-2Cu Maraging Steels, *Acta Mater.*, 1998, **46**, p 6063
20. C.N. Hsiao, C.S. Chiou, and J.R. Yong, Aging Reactions in a 17-4 PH Stainless Steel, *Mater. Chem. Phys.*, 2002, **74**, p 132
21. V.I. Dimitrov, J. Dhaen, G. Knuyt, C. Quaeyhaegens, and L.M. Stals, A Method for Determination of the Effective Diffusion Coefficient and Sputtering Rate During Plasma Diffusion Treatment, *Surf. Coat. Technol.*, 1998, **99**, p 23
22. E. Menthe and K.-T. Rie, Further Investigation of the Structure and Properties of Austentic Stainless Steel After Plasma Nitriding, *Surf. Coat. Technol.*, 1999, **116–119**, p 199